A decomposition method for the fast computation of the transmission error of gears with holes

Youness Benaicha, A Mélot, Emmanuel Rigaud, J-D Beley, Fabrice Thouverez, Joël Perret-Liaudet

A decomposition method for the fast computation of the transmission error of gears with holes

Y. Benaïcha[a,b,*], A. Mélot[a], E. Rigaud[a], J-D. Beley[b], F. Thouverez[a] and J. Perret-Liaudet[a]

[a]Univ Lyon, Ecole Centrale de Lyon, ENISE, ENTPE, CNRS, Laboratoire de Tribologie et Dynamique des Systèmes LTDS, UMR 5513, F-69134, Ecully, France
[b]ANSYS SAS, 35-37 rue Louis Guérin, 69100 Villeurbanne Cedex, France

ARTICLE INFO

Keywords:
Gear transmission error
Flexible multibody modelling
Decomposition method
Spur gear with holes
Gear body design

ABSTRACT

The prediction of noise and vibrations generated by geared systems remains a challenging field of study. The analysis of such systems is computationally demanding mainly due to the large size of the finite element model used to describe the system and the nonlinear behaviour arising from the contact between the gear teeth. As a consequence, very few models have been proposed to handle lightweight gears which are widespread in current industrial designs. Lightweight gears lead to a strong modification of the gear compliance, and therefore the contact force distribution. The static transmission error and the mesh stiffness fluctuations are thus influenced by these changes. In this paper, a 2D decomposition method is proposed to compute the static transmission error of gears with holes in the gear blanks without heavy computational effort. The original methodology relies on the substructuring of the holed gear blank from the gear teeth. It is applied on several spur gear systems with holed gear blanks and compared with a fully flexible multibody method. The validity of the approach is assessed in terms of static transmission error and mesh stiffness fluctuations. Moreover a parametric study is carried out using the 2D decomposition method in order to analyse the influence of holes regarding their position and number.

1. Introduction

The issues related to energy consumption and air pollution have increased the need for on-board mass reduction. This requirement concerns in particular drivelines equipped with gear transmissions. The proposed solutions to decrease the gear mass consists in using composites [6, 7] or removing material from the gear blanks by employing thin rim or holes [16]. This paper focuses on the specific relevance of introducing holes in the gear blanks. However, mass reduction may compromise the integrity of the structure and the vibroacoustic performances. Thus, it is of paramount importance to verify that adding holes does not increase the gear mesh excitation and the resulting whining noise. It is well-known that the main excitation source generated by the gear operation is the static transmission error (STE). It generates dynamic mesh forces which are transmitted to the housing through wheel bodies, shafts and bearings. Housing vibratory state is related to the radiated whining noise [5]. The STE is defined as the difference between the actual position of the driven gear and the position it would occupy if the gear pair were perfectly conjugate [24]. It can be expressed along the gear line of action as $\delta(\theta_1)$:

$$\delta(\theta_1) = R_{b2}\theta_2 - R_{b1}\theta_1 \tag{1}$$

where θ_1 and θ_2 are respectively the angular position of the driving wheel with Z_1 teeth and the driven wheel with Z_2 teeth. The STE stems from manufacturing errors (unintended modifications), micro-geometry deviations (intended modifications) and tooth deformations. These deformations arise from local tooth contact (hertzian-like deformation), tooth bending and shear, and global deformation which induces shafts misalignment and modifies the location of the contact lines. If we assume identical teeth, axisymmetric gear bodies, no eccentricity and no pitch errors, the STE exhibits periodic fluctuation at the mesh frequency f_m. If only one wheel presents eccentricity defect or a holed gear blank, the fundamental frequency corresponds to the rotating frequency of the considered wheel f_1 or f_2. If both driving and driven wheels have eccentricity defects or holes, the fundamental frequency of the STE f_0 is associated to

*Corresponding author
youness.benaicha@ec-lyon.fr (Y. Benaïcha)
ORCID(s):

the period T_0 needed to re-establish contact between a particular tooth of the driving wheel and a particular tooth of the driven wheel.

$$f_0 = \frac{1}{T_0} = \frac{f_m}{Z_1 Z_2} = \frac{f_1}{Z_2} = \frac{f_2}{Z_1} \tag{2}$$

Nomenclature

Matrices and vectors

$\mathbf{1}$	Unity column vector
$\mathbf{e}(\theta_1)$	Initial gap vector
$\mathbf{u}$	Vector of generalized displacements
$\mathbf{p}(\theta_1)$	Distributed load
$\mathbf{C}$	Damping matrix
$\mathbf{H}(\theta_1)$	Symmetric semi-positive compliance matrix
$\mathbf{K}$	Stiffness matrix
$\mathbf{M}$	Mass matrix
$\mathbf{F}_{ext}$	Vector of external force
$\mathbf{F}_{nl}$	Vector of nonlinear force

Scalars

α	Pressure angle
$\delta(\theta_1)$	Static transmission error
ϵ	Gap criteria
κ	Penalty stiffness coefficient
λ	Lagrange multiplier
ϵ_α	Contact ratio
$k(\theta_1)$	Mesh stiffness
m	Gear module
a	Center distance
b_f	Face width
f_m	Mesh frequency
g	Gap distance
h_a	Addendum
h_d	Dedendum
r_h	Radius of holes
x	Profil shift coefficient
A_m	Amount of tip relief modification
L	Length of tip relief modification
F	Transmitted load
T	Output torque
H_n	Harmonic orders
N_h	Number of holes
R	Radial position of holes
R_b	Base radius
Z	Number of teeth

Subscripts and superscripts

ed	Edge
h	Holes
in	Inside
gb	Gear blank
wh	Without holes

Abbreviations

DoF	Degree of freedom
FE	Finite element
NVH	Noise, vibration and harshness
STE	Static transmission error
STE_{pp}	Peak-to-peak STE amplitude

The STE is also responsible for an internal parametric excitation associated with the mesh stiffness fluctuation

$k(\theta_1)$. It exhibits the same frequency components as the STE fluctuation. For each driving angular position θ_1, the mesh stiffness is defined as the derivative of the transmitted load F relative to the STE $\delta(\theta_1)$ [5]:

$$k(\theta_1) = \frac{\partial F}{\partial \delta(\theta_1)} \tag{3}$$

Classical approaches used to compute the static transmission error and the mesh stiffness fluctuations are based on the equation describing the static equilibrium of the gear pair for a set of successive positions of the driving wheel θ_1. The contact is assumed to occur on the theoretical contact lines which are identified thought a kinematic analysis of the system [1, 3, 17, 28]. The gear tooth flexibility is described using a compliance matrix $\mathbf{H}(\theta_1)$ obtained with finite element or semi-analytical models [9]. The hertzian-like local deformation is taken into account thanks to additional contributions deduced from Hertz theory and added to $\mathbf{H}(\theta_1)$. Tooth flank modifications and manufacturing errors are introduced as an initial gap $\mathbf{e}(\theta_1)$ between the discretized contact lines. Misalignment and deviation induced by the global deformation of the entire gear train are introduced at this stage. For each position θ_1 and for a given transmitted normal load F, the equation describing the gear mesh contact is formulated in matrix form as follows:

$$\begin{cases} \mathbf{H}(\theta_1).\mathbf{p}(\theta_1) = \delta(\theta_1).\mathbf{1} - \mathbf{e}(\theta_1) \\ \mathbf{1}^T.\mathbf{p}(\theta_1) = F \end{cases} \tag{4}$$

with:

$$\begin{cases} \sum_j H_j(\theta_1) p_j(\theta_1) + \delta(\theta_1) \geq e_j(\theta_1) \\ p_j \geq 0 \end{cases} \tag{5}$$

In this constrained problem, the column vector $\mathbf{1}$ has all its components equal to 1, the column vector $\mathbf{p}$ and the scalar function $\delta(\theta_1)$ are respectively the unknown distributed load and the unknown STE. The solutions $\mathbf{p}(\theta_1)$ and $\delta(\theta_1)$ are obtained using an optimization method. For instance, a modified simplex method was used by Conry *et al.* in [8]. Some authors studied the influence of an elastic gear body on the tooth flexibility and the STE fluctuation. Weber and Banascheck [23] proposed a model to estimate the gear body-induced tooth deflection. The tooth is assumed to be rigid and the wheel body is modeled as an elastic half plane. Sainsot [18] extended the previous model by developing a semi-analytical formula for which the elastic half plane is replaced by a solid disk. The assumptions behind these methods entail an overestimation of the mesh stiffness. Rigaud *et al.* [17] assessed the influence of cylindrical and thin-rimmed elastic gear bodies on the STE. For cylindrical gear bodies, they reported a modification of the mean value without significant influence on the fluctuation. However, designing thin-rimmed gear bodies and taking into account interactions between adjacent teeth lead to a modification of both the mean value and the fluctuation of the STE.

Some improvements have been made in the last few years in order to include lightweight gear bodies in the static transmission error analysis. Guilbert *et al.* [11, 12, 13] proposed a condensed finite element sub-structure connected to a lumped parameter model. They paid attention to the mesh interface model to connect a lumped parameter with a FE model. The contact occurs on the theoretical contact lines and the flexibility of the gear teeth is described through several independent stiffness distributed along the line of action. The effects of a thin rim wheel or holes in the gear blanks were assessed [10]. The presence of holes modulates the STE. Additionally, Shweiki [19] used several nonlinear FE simulations with high detailed model of the meshing gears to estimate the STE fluctuations. Cappellini [4] and Shweiki [20] also combined a FE approach and an analytical representation of the gear mesh stiffness to investigate the behaviour of lightweight gears. The total deformation of the gear induced by the gear mesh contact is modelled as a global contribution coming from the tooth deflection, mainly bending and shear, and a local nonlinear hertzian-like deformation. Active tooth pair are divided into multiple slices along the width and the contact points are considered to lie on the rigid involute profile. They also decreased the computation time of the global deformation by performing a model order reduction obtained from a series of linear static analyses where a normal load is applied on selected nodes belonging to theoretical contact lines [4]. Hou *et al* [14] investigate the effect of thin rimmed gears on the NVH performance. As Rigaud they show that thin rim in the gear blanks modifies the mean and the peak-to-peak value of the STE. This modification is used to optimize the thin-rimmed gears and to reduce the gear mass about 25% and the dynamic mesh forces about 68%. Moreover, a recent fully flexible multibody approach has been proposed to compute the STE for any kind of gears, especially gears with thin rim bodies or holes [2]. It consists of a complete FE model without restrictive assumptions concerning the mesh contact. A FE-based contact with a surface-to-surface detection and an augmented lagrange multiplier formulation is used. The proposed model is enabled to detect additional

frequency components induced by the presence of holes in the gear blanks. Among previous works, the most advanced strategies allow the computation of the transmission error of gears with holes but, when no assumption are made on the contact detection phase, the simulation requires a large computational effort to perform the analysis over a fundamental period of the STE. Simulations can last for several days due to the nonlinearity and the large number of degrees-of-freedom. Parametric studies become prohibitive.

The approach proposed in this paper aims at overcoming the time cost limitation while preserving a multibody formulation. It consists in separating the gear body deformation and the tooth deformation when computing the transmission error. The periodic displacement field of the gear body with holes is computed by transmitting and enforcing instantaneous operating contact conditions at the gear body edge. The approach offers significant improvements in terms of computing time compared with a fully multibody approach. The behaviour of a large variety of lightweight gears can be thus assessed through parametric studies. The STE and the mesh stiffness fluctuations are the physical quantities used to validate the proposed methodology.

The paper is structured as follows: first, the flexible multibody approach used as the reference model is briefly described in section 2. The 2D decomposition procedure is detailed in section 3. Then the novel methodology is validated by comparing the results with those obtained with the fully flexible multibody approach in section 4. Finally, the effect of number and radial position of holes is evaluated by carrying out a parametric study.

2. Flexible multibody model

This section presents the original elastic multibody formulation recently proposed in [2] which is used as the reference model. The flexible multibody model solves a frictionless contact problem within the FE method. Indeed, gear bodies including teeth are discretized by FE method. The mesh is refined in the contact area with linear hexahedron elements.

In this paper, the approach is used in 2D. The FE-based contact between the gear teeth is solved by using a surface-to-surface algorithm. The surface-to-surface contact detection prevents the interpenetration of the target body into the contact body. No a priori assumptions are made concerning the gear contact existence and location. The contact problem is modelled with an augmented lagrangian formulation [15, 21]. This description is a compromise between lagrange multiplier and penalty methods, which enables a mastered enforcement of the impenetrability constraint while improving the convergence of the algorithm. The mathematical formulation of the noonsmooth mechanics is given by the Signorini conditions [25, 26, 27]:

$$\begin{cases} g_i \geq 0 \\ F_i \geq 0 \\ g_i F_i = 0 \end{cases} \qquad \forall i, \tag{6}$$

Gap function g_i is associated to every contact node i and corresponds to the distance between the contact and the target surfaces along the normal direction. F_i is the contact force acting on the target surface. It is expressed as:

$$F_i^j = \kappa g_i^j + \lambda_i^j \tag{7}$$

κ is the penalty stiffness coefficient set to 10^{17}, λ_i^j is the iterative lagrange multiplier at the iteration j associated to the contact node i which is updated until the gap function g_i^j is sufficiently small (i.e $d_i^j \leq \epsilon$, typically $\epsilon = 10^{-2}$) [15, 21]. Equation (6) implies that all contacts must be compressive. The constraints $g_i \geq 0$ and $g_i F_i = 0$ represent the impenetrability and complementarity conditions. The contact forces $F_i \geq 0$ are generated only when the gear tooth contact occurs ($g_i = 0$), while the contact forces are zero ($F_i = 0$) when the gear tooth contact is lost ($g_i > 0$).

These Signorini conditions are then included in the discretized equation of motions of the gear pairs. Formally, the equation of motion for the gear dynamics is expressed as follows:

$$\mathbf{M\ddot{u}} + \mathbf{C\dot{u}} + \mathbf{Ku} + \mathbf{F}_{nl}(\mathbf{u}) = \mathbf{F}_{ext} \tag{8}$$

where $\mathbf{u}$ contains the generalised displacement of each degree-of-freedom and $\mathbf{M}$, $\mathbf{C}$, $\mathbf{K}$ are respectively the mass, damping and stiffness matrices. $\mathbf{F}_{ext}$ is the vector of external forcing. In order to access to the static transmission

error, the multibody gear simulation is performed in the quasi-static regime by setting a low rotation speed of the driving gear (1 rpm) using the ANSYS Mechanical ® solver. The analysis is structured as follows:

- firstly, the gear backlash is covered by a rotation of the driving wheel in order to establish the contact at an initial state,
- then, the output torque is applied to the driven wheel while maintaining the driving wheel,
- finally, a rotation of the driving wheel is performed over a period corresponding to the fundamental period of the static transmission error.

Control nodes are defined at each gear centre to apply boundary conditions and to measure the time varying driving and driven gear angles (θ_1, θ_2). The static transmission error $\delta(\theta_1)$ is then computed along the line of action and the mesh stiffness $k(\theta_1)$ is approximated by a numerical differentiation of the transmitted load F versus $\delta(\theta_1)$. The contact procedure used in the flexible multibody approach is summarized in Fig. 1.

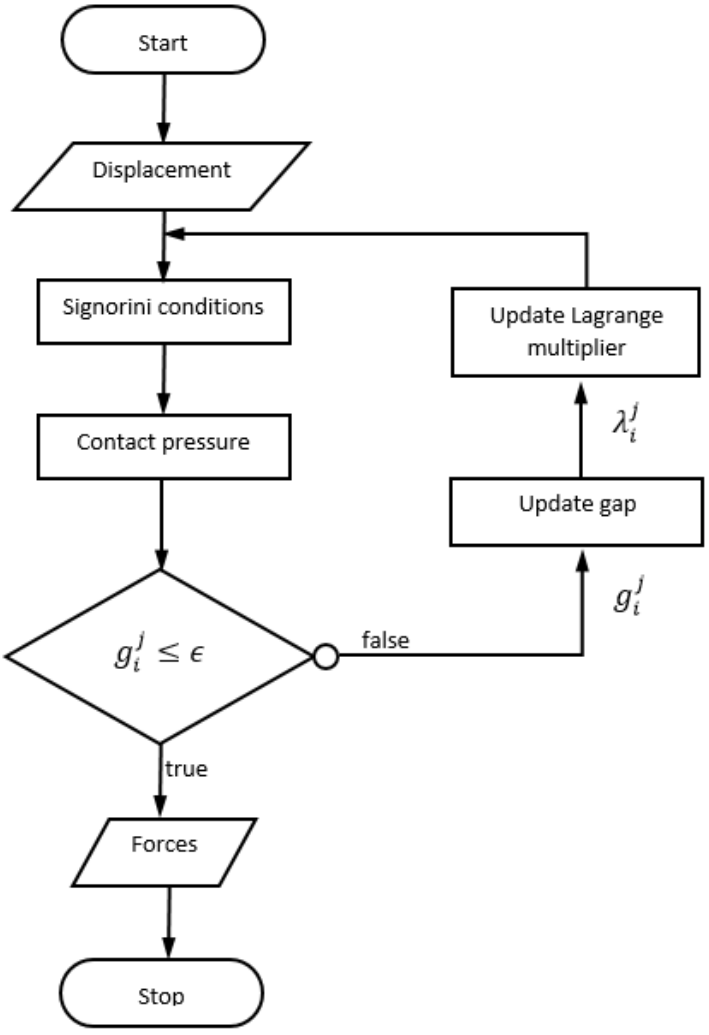

Figure 1: Flow chart of the contact procedure

The procedure can be applied to a gear pair with holes in the gear blanks. However, the fundamental frequency of the STE no longer corresponds to the mesh frequency f_m because the fundamental frequency f_0 is decreased due

to the presence of holes. This phenomenon leads to time consuming simulations. It thus becomes difficult to conduct parametric studies at the design stage. In this context, an original decomposition method is proposed in order to reduce the computational time cost while preserving numerical accuracy. The next section presents, assesses and discusses the decomposition method.

3. The proposed original decomposition method for gears with holes

This section describes the strategy used to decompose the deformation of the gear body with holes and the deformation induced by the contact between gear teeth. The proposed method is mostly based on the assumption that the tooth deflection is not coupled to the deformation of the gear body, so that its behaviour can be accounted for with an additional flexibility. The following developments present the substructuring of gears with identical and equidistant holes in the gear blanks. The objective is to estimate the instantaneous deformation of the holed gear blank and the gear teeth. The system is decomposed into two substructures as shown in Fig. 2. The first one referred to as "gb", represents only the elastic holed gear body with a radius R_w. The second one, labelled "wh", is the complementary part of the gear pair where the holed gear blank is replaced by a rigid wheel.

The decomposition method presented in this section takes only into account rotation around shaft axis which means that a possible twist of the tooth flank in the plane of action is neglected. This constitutes the main limitation of the proposed method, although it can be extended to 3D rotations with additional research. It still provides a significant computational time reduction when studying gears without thin-rimmed bodies.

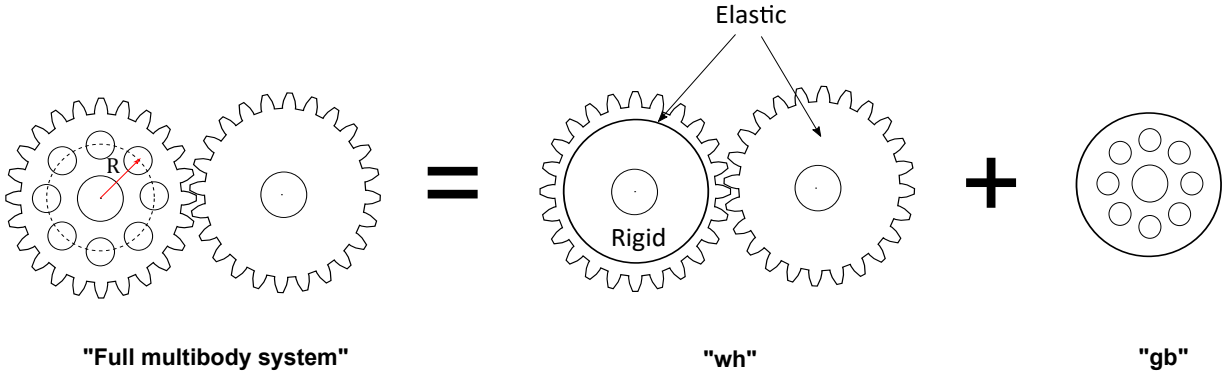

Figure 2: Decomposition of gear pair with holes

The decomposition method is thus structured as follows:

- Firstly, the flexible multibody approach described in section 2 is applied to the second substructure "wh". For this substructure, the simulation is performed over one mesh period since the holed gear blank is not considered. The substructure is discretized by the FE method. The equation of motion of substructure "wh" is expressed as follows:

$$\mathbf{M}_{wh}\ddot{\mathbf{u}}_{wh} + \mathbf{C}_{wh}\dot{\mathbf{u}}_{wh} + \mathbf{K}_{wh}\mathbf{u}_{wh} + \mathbf{F}^{nl}_{wh}(\mathbf{u}_{wh}, \theta_1) = \mathbf{f}^{ex}_{wh} \tag{9}$$

  The resulting static transmission error named $\boldsymbol{\delta}_{wh}(\theta_1)$ is:

$$\delta_{wh}(\theta_1) = R_{b2}\theta_2^{wh} - R_{b1}\theta_1^{wh} \tag{10}$$

  θ_1^{wh},θ_2^{wh} are respectively the angular displacement measured at the centre of the driving and driven gears.

- Next, the quasi-static motion of the full multibody system shown in Fig 2 corresponding to an amplitude $2\pi/N_h$ is discretized in 16 angular positions. For each angular position, the fully multibody method is applied and the tangential displacement field at the interface between "wh" and "gb" is extracted. This displacement is then introduced as an imposed displacement on the substructure "gb" while applying the output torque at the

centre. Considering $\mathbf{u}_{gb}^{in}$ and $\mathbf{u}_{gb}^{ed}$, the displacements of the DoF located inside and at the interface of "gb", the deformation of "gb" is obtained by using the static relationship:

$$\begin{bmatrix} \mathbf{K}_{in,in} & \mathbf{K}_{in,ed} \\ \mathbf{K}_{ed,in} & \mathbf{K}_{ed,ed} \end{bmatrix} \begin{pmatrix} \mathbf{u}_{gb}^{in} \\ \mathbf{u}_{gb}^{ed} \end{pmatrix} = \begin{pmatrix} \mathbf{f}_{gb}^{in} \\ \mathbf{0} \end{pmatrix} \tag{11}$$

So,

$$\mathbf{u}_{gb}^{in}(\theta_{1,2}) = \mathbf{K}_{in,in}^{-1}(\mathbf{f}_{gb}^{in} - \mathbf{K}_{in,ed}\mathbf{u}_{gb}^{ed}(\theta_{1,2})) \tag{12}$$

For each angular position, the angular deformation at the centre of "gb" referred to as $\theta^{gb}(\theta_{1,2})$ is retrieved. We assume that this displacement is periodic at $2\pi/N_h$. $\theta^{gb}(\theta_{1,2})$ is thus formulated as a trigonometric function:

$$\theta^{gb}(\theta_{1,2}) = A + B\cos\left(\frac{2\pi\theta_{1,2}}{N_h}\right) \tag{13}$$

The curve is displayed in Fig. 3.

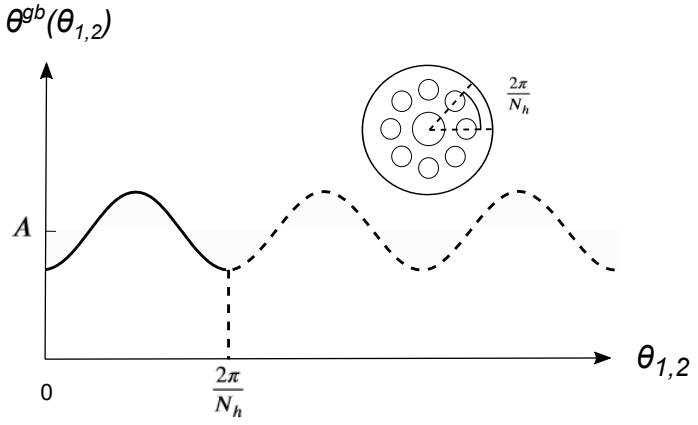

Figure 3: Angular deformation retrieved at the centre of "gb"

The resulting contribution along the line of action of the gear body with holes $\delta_{gb}(\theta_{1,2})$ is defined as:

$$\delta_{gb}(\theta_{1,2}) = R_b\theta^{gb}(\theta_{1,2}) \tag{14}$$

- Finally, substructures "wh" and "gb" allow the computation of the deflection $\delta_{wh}(\theta_1)$ and $\delta_{gb}(\theta_1)$, respectively. The static transmission error of the gear pair with holes $\delta_h(\theta_1)$ is computed as:

$$\delta_h(\theta_1) = \delta_{wh}(\theta_1) + \delta_{gb}(\theta_{1,2}) \tag{15}$$

The mesh stiffness of the gear pair with holes $k_h(\theta_1)$ is obtained with a numerical differentiation of the transmitted load F versus $\delta_h(\theta_1)$, according to eq. (3).

The decomposition procedure allows the computation of the STE for a large variety of holed gear blanks. The computational time reduction comes from the fact that it is not necessary to solve the gear mesh contact over a fundamental period of the STE. The estimation of the deformation of the holed gear blank apart of the full multibody system is the key. It permits to keep the resolution of the nonlinear analysis over a mesh period. Figure 4 outlines the decomposition procedure, which can be extended to deal with a gear pair design with holes in both gear blanks by adding another substructure.

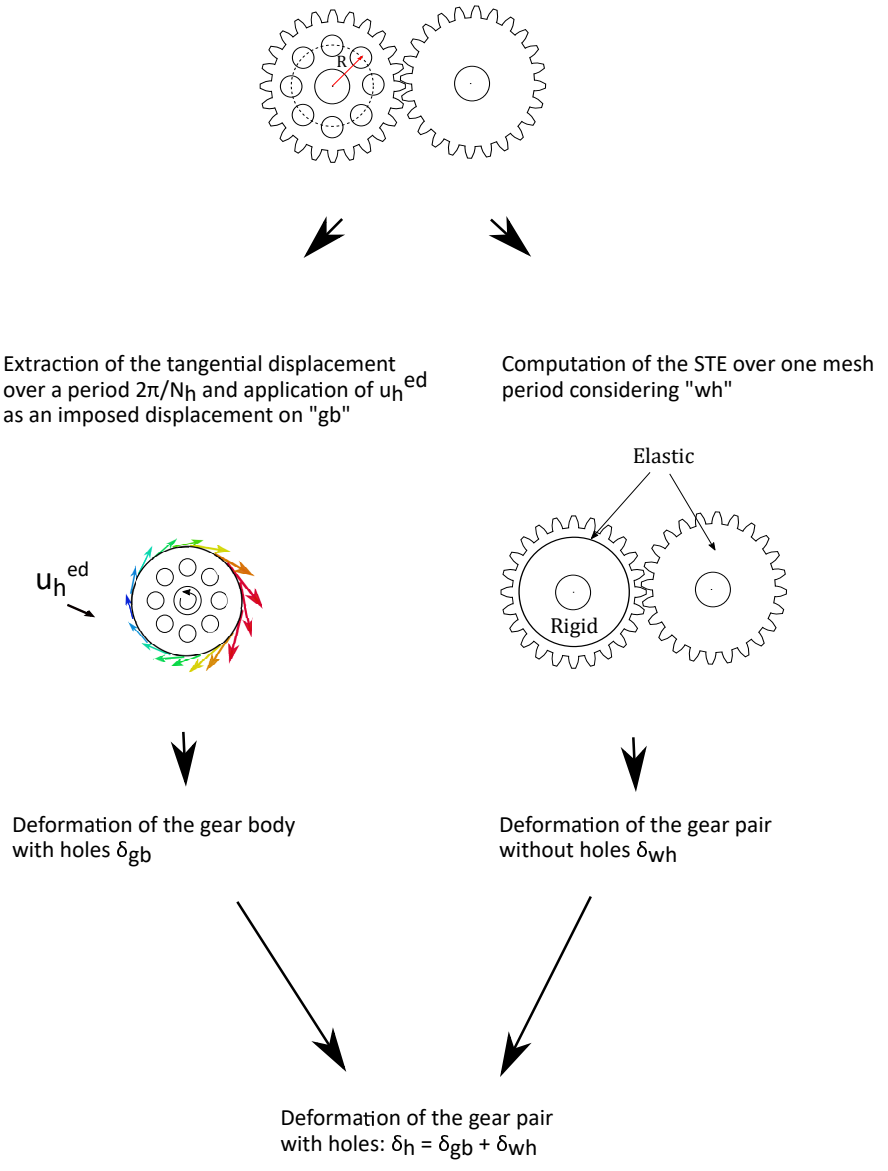

Figure 4: Flow chart of the decomposition procedure

4. Numerical validations

The decomposition procedure is applied on three different test cases in order to show the large variety of gears that can be analyzed. The STE and mesh stiffness fluctuations are validated by comparing results with those obtained using the fully flexible multibody simulation described in section 2.

4.1. Decomposition procedure applied to different test cases

The gear characteristics of the different test cases are presented in Table 1. The first corresponds to a reverse gear pair with the same number of holes in the driving and driven wheels. The second corresponds to a gear pair with holes only in the driven wheel. The third corresponds to a reducer gear pair with holes only in the driven wheel. Designs of the different test cases are shown in Fig. 5. Gear pairs have also intentional removal of material along the tooth profile corresponding to a linear tip relief with length $L = 1.75\,\text{mm}$ and amount $A_m = 5\mu\text{m}$. This micro-geometric tooth modification is introduced to minimize the STE for an output torque $T = 115\,\text{N m}$ for the reverse gear pairs and

$T = 160\,\mathrm{N\,m}$ for the reducer gear pair.

Name	Designation	Case 1		Case 2		Case 3		Unit
-	-	Gear 1	Gear 2	Gear 1	Gear 2	Gear 1	Gear 2	-
Module	m	2		2		2		mm
Number of teeth	Z	50	50	50	50	29	85	-
Pressure angle	α	20		20		20		deg
Base radius	R_b	46.984	46.984	46.984	46.984	27.251	79.874	mm
Profile shift coefficient	x	0	0	0	0	0	0	-
Addendum	h_a	2	2	2	2	2	2	mm
Dedendum	h_d	2.5	2.5	2.5	2.5	2.5	2.5	mm
Face width	b_f	20	20	20	20	20	20	mm
Center distance	a	100.5		100.5		118.5		mm
Tip relief modification								
Length	L	1.75	1.75	1.75	1.75	1.75	1.75	mm
Amount	A_m	5	5	5	5	5	5	μm
Lightweighting								
Number of holes	N_h	8	8	-	10	-	6	-
Radius of holes	r_h	10	10	-	7.5		17.5	mm

Table 1: Gear characteristics of the different test cases

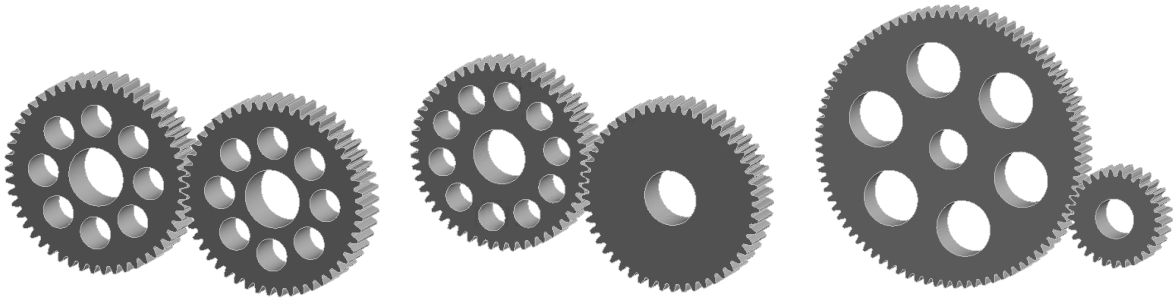

(a) (b) (c)

Figure 5: Test case 1: (a) reverse gear pair with 8 holes on driving and driven gears. Test case 2: (b) reverse gear pair with 10 holes closer to the teeth on the driven gear only. Test case 3: (c) reducer gear pair with 6 holes.

Figures 6, 7 and 8 displays the time evolutions and the amplitude spectra of STE and mesh stiffness for the three test cases. The harmonic orders H_n are identified with respect to the output frequency. Amplitude spectra of STE and mesh stiffness show components at the mesh frequency H_{Z_2} and its harmonics H_{kZ_2}. They also show component at harmonic H_{N_h} induced by holes designed in the driven wheel. For the reverse gear corresponding to the test case with holes in the driving gear, no additional component is observed because the number of holes is the same as those of the driven wheel. Amplitudes of components are identical for the fully elastic multibody method and the decomposition method.

Spectra also show sidebands around harmonics of the mesh frequency, $H_{kZ_2 \pm lN_h}$, for the fully elastic multibody simulation because the number of holes N_h is not a submultiple of the number of teeth Z_2, but their amplitudes are negligible compared to those of H_{N_h} and H_{kZ_2}. These sidebands are not observed for the STE spectra computed with the decomposition method. Nevertheless, they arise from the mesh stiffness spectra because this one is computed from a numerical differentiation of the transmitted load F relative to STE, according to eq. (3).

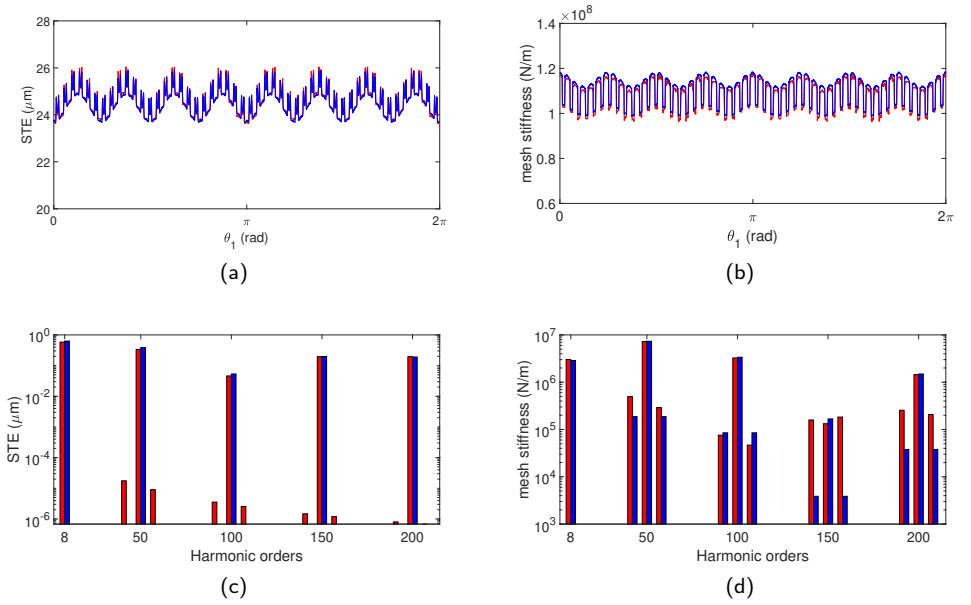

Figure 6: Test case 1: time evolution of the STE (a) and the mesh stiffness (b) for an output torque $T = 115\,\mathrm{N\,m}$. Amplitude spectrum of STE fluctuation (c) and mesh stiffness fluctuation (d). —decomposition method, —fully flexible multibody method

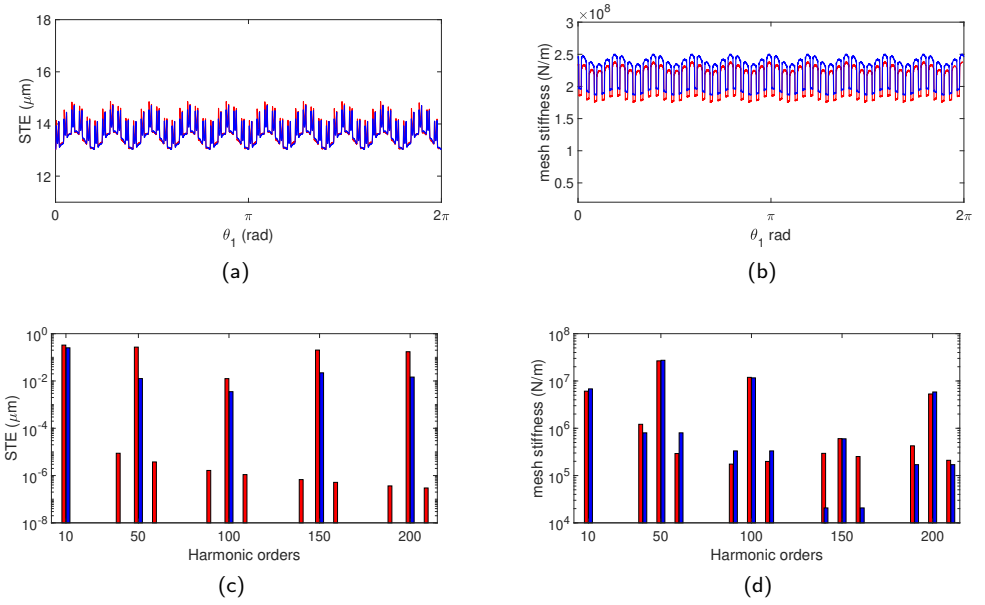

Figure 7: Test case 2: time evolution of the STE (a) and the mesh stiffness (b) for an output torque $T = 115\,\mathrm{N\,m}$. Amplitude spectrum of STE fluctuation (c) and mesh stiffness fluctuation (d). —decomposition method, —fully flexible multibody method

Finally, Fig. 6, 7 and 8 confirm that the results obtained with the decomposition method are similar to those obtained with the fully flexible multibody approach. Shapes of time evolutions, mean and root mean square values and peak to peak amplitude are very close as reported in Table 2.

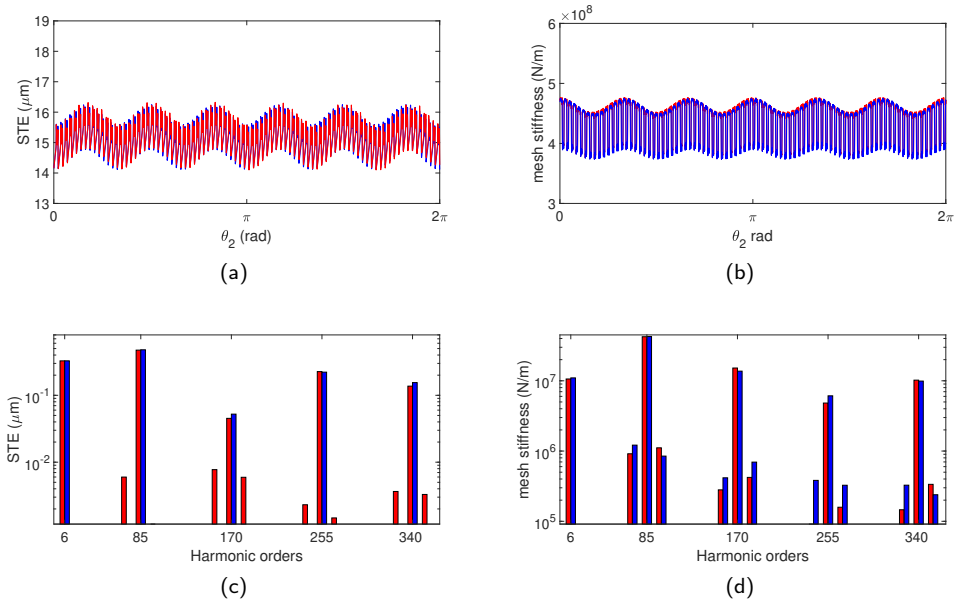

Figure 8: Test case 3: time evolution of the STE (a) and the mesh stiffness (b) for an output torque $T = 115\,\mathrm{N\,m}$. Amplitude spectrum of STE fluctuation (c) and mesh stiffness fluctuation (d). —decomposition method, —fully flexible multibody method

Test case 1	Fully flexible multibody method	Decomposition method	Error (%)	Unit
STE mean value	24.587	24.534	0.2	μm
STE rms value	0.572	0.523	8.5	μm
STE peak-to-peak amplitude	2.408	2.216	8	μm
mesh stiffness mean value	1.088e8	1.103e8	1.4	N/m
mesh stiffness rms value	6.358e6	6.356e6	0.03	N/m
mesh stiffness peak-to-peak amplitude	2.101e7	1.984e7	5.5	N/m
Test case 2	Fully flexible multibody method	Decomposition method	Error (%)	Unit
STE mean value	13.651	13.587	0.5	μm
STE rms value	0.418	0.365	12	μm
STE peak-to-peak amplitude	1.843	1.688	8.4	μm
mesh stiffness mean value	2.130e8	2.239e8	5	N/m
mesh stiffness rms value	2.210e7	2.263e7	2.4	N/m
mesh stiffness peak-to-peak amplitude	6.367e7	6.394e7	0.4	N/m
Test case 3	Fully flexible multibody method	Decomposition method	Error (%)	Unit
STE mean value	15.103	15.093	0.1	μm
STE rms value	10.468	0.466	0.4	μm
STE peak-to-peak amplitude	2.222	2.129	4.4	μm
mesh stiffness mean value	4.347e8	4.325e8	0.5	N/m
mesh stiffness rms value	3.456e7	4.345e7	1.5	N/m
mesh stiffness peak-to-peak amplitude	1.017e8	1.018e8	0.1	N/m

Table 2: STE and mesh stiffness comparisons between the fully flexible multibody method and the decomposition method

4.2. Time cost reduction

Comparisons of STE and mesh stiffness fluctuations for the different test cases prove the accuracy of the decomposition method. Besides, high computational resources are required to compute STE and mesh stiffness fluctuations with a fully flexible multibody method. Indeed, the method requires a fine mesh for all the gear teeth and 40 computation points over a mesh period, which means that $40 \times Z_2$ final computation points are used to describe precisely the STE. On the other hand, for the decomposition method, only teeth covering the angle $2\pi/N_h$ need a fine mesh and 16 computation points are retained to reconstruct the trigonometric angular deformation of the substructure "gb". Moreover, 40 computation points are added to the latter for the computation of the STE of the substructure "wh". As a consequence, with the fully multibody method, the elapsed computing time is 15 hours for the reverse gear pair and 40 hours for the reducer. Whereas, for the decomposition method, 30 minutes (30 times faster) are needed for the reverse gear pair and 40 minutes (60 times faster) for the reducer.

5. A parametric study of the effect of number and radial position of holes in gear blanks

The time cost reduction associated with the decomposition procedure allows parametric analysis. In the following section, the objective is to analyze the influence of number and radial position of holes on the static transmission error and mesh stiffness fluctuations.

5.1. Problem statement

A standard gear without holes is considered as a reference test case. It consists of a spur gear with characteristics $Z_1 = Z_2 = 50$, $m = 2\,\text{mm}$, $\alpha = 20°$, $b_f = 20\,\text{mm}$ and $a = 100.5\,\text{mm}$. A tip relief modification with amount $A_m = 5\mu\text{m}$ and length $L = 1.75\,\text{mm}$ is introduced in the tooth profile to smooth the gear meshing. It leads to a minimization of the STE fluctuation for an operating output torque $T_{opt} = 115\,\text{N m}$. Fig. 11 shows that the corresponding peak-to-peak amplitude is $STE_{pp} = 1\mu\text{m}$. Fig. 10 shows that the peak-to-peak amplitude is larger for a lower output torque ($STE_{pp} = 2\mu\text{m}$ for $T_{low} = 20\,\text{N m}$). Then, the holed configurations are created from the standard gear by designing holes in the driven gear body to reduce the gear mass by 25% as presented in the Fig 9. For instance, a configuration with N_h eight holes at a radial position $R = 34\,\text{mm}$ from the centre of the gear is labelled 8R34. A holed gear blank is introduced only for the driven gear to reduce the number of suitable configurations. The size of holes is defined to maintain a constant mass for all designed gear pairs. The radial position and the number of holes are chosen to preserve the structural integrity of the gear pair. The selected gears are then labelled by (✓) and notified in Table 3.

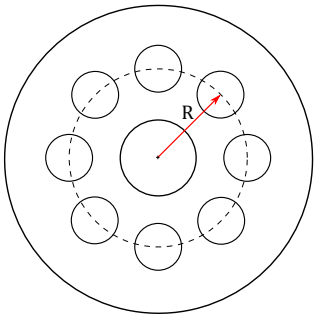

Figure 9: Schematic representation of the holed configuration

R (mm) \ N_h	6	8	10
27	✗	✓	✗
30	✓	✓	✗
34	✗	✓	✓

Table 3: Gear pairs with holes retained according to the number of holes N_h and their radial position R

5.2. Effect of number and radial position of holes

The decomposition procedure is applied on the previous configurations for a low output torque $T_{low} = 20\,\text{N m}$ and an optimal output torque $T_{opt} = 115\,\text{N m}$ established for the standard gear pair.

As expected and compared with the standard gear pair, Fig. 10 and Fig. 11 show that STE and mesh stiffness fluctuations present an additional low frequency component H_{N_h} for all the other configurations. The amplitude of this component H_{N_h} is related to the number of holes N_h, their radial position R and the output torque value considered.

The effect of the radial position of holes is illustrated by the cases "8R34", "8R30" and "8R27". Indeed, Fig. 10 and Fig. 11 show that the amplitude of the component H_{N_h} is larger when the radius R is increased, which means when the holes are close to the tooth root radius.

The effect of the number of holes is illustrated by the pair cases ("10R34", "8R34") and ("8R30", "6R30"). Figures 10 and 11 show for a given radial position of holes that increasing the number of holes reduces the STE fluctuations.

The effect of the output torque is also significantly identified. STE fluctuations of the standard gear pair are governed by the micro-geometry modification for a low output torque $T_{low} = 20\,\text{N m}$. Whereas STE fluctuations are governed by the gear deformation for the optimal output torque $T_{opt} = 115\,\text{N m}$. The amplitude of the low frequency fluctuations associated with the H_{N_h} component is thus increased.

The critical modes for which the strain energy at the gear mesh is the highest are governed by the mean value of the mesh stiffness. Designing holes in the gear blanks decreases the mean value and the fluctuations of the mesh stiffness (Fig. 10 and Fig. 11). As a consequence, the critical frequencies are reordered. The fluctuations of the mesh stiffness are modified compared to the standard gear pair. These changes have thus important influence on the parametric resonances observed for the dynamic response [22].

6. Conclusion

Designing lightweight gears through the use of holed gear blanks is widespread in industries. It helps engineers to reach their mechanical and environmental requirements, which are mainly mass reduction and increase operating speed. However, the structural integrity has to be preserved.

This paper proposes a 2D decomposition procedure based on the substructuring of the holed gear bodies and the remainder of the gear pair. The approach bypasses the computation of the full nonlinear multibody system while considering the contribution of holes. The efficiency of our approach was assessed by considering the fully multibody approach as a reference for the computation of static transmission error and the mesh stiffness fluctuations. The decomposition procedure reduces considerably the elapsed computing time, which enables fast parametric studies of gears with holes. Thanks to a parametric study, this work features the effects of holed gear blanks on the static transmission error and the mesh stiffness fluctuations. It shows that different effects appear according to the radial position and number of holes and the output torque considered. An additional low frequency component corresponding to the existence of holes is observed. Then, the amplitude of the component H_{N_h} is increased with the operating output torque and with the radial position R. On the other hand, increasing the number of holes for a given radial position R, reduce the STE fluctuations. The mean values of the different mesh stiffness are reduced compared with the standard gear pair and the fluctuations are significantly modified. Holes in gear blanks can be thus a design strategy to reduce the mesh stiffness mean value and fluctuations. The observed effects cannot be set apart because they have important consequences on the parametric and dynamic responses.

Our ongoing research focuses on the extension of the 2D decomposition method to 3D in order to deal with helical gears with thin-rimmed bodies and holes in the gear blanks. 3D rotations will be quantified and added to the decomposition procedure in order to consider possible twist of the gear body.

Acknowledgements

The authors would like to thanks ANSYS and the ANRT (French National Association for Research and Technology) for their support via a CIFRE grant. This work was performed within the framework of the LabCom LADAGE (LAboratoire de Dynamique des engrenAGEs), created by the LTDS and the Vibratec Company and operated by the French National Research Agency (ANR-14-LAB6- 0003). It was also performed within the framework of the LABEX CeLyA (ANR-10-LABX-0060) of Université de Lyon, within the program « Investissements d'Avenir » (ANR-16-IDEX-0005) operated by the French National Research Agency (ANR).

Conflict of interest

The authors declare that they have no conflict of interest.

References

[1] Andersson, A., Vedmar, L., 2003. A dynamic model to determine vibrations in involute helical gears. Journal of Sound and Vibration 260(2), 195–212.

[2] Benaïcha, Y., Perret-Liaudet, J., Beley, J., Rigaud, E., Thouverez, T., . On a flexible multibody modelling approach using FE-based contact formulation for describing gear transmission error. 2021, hal-03178317 .

[3] Cai, Y., 1995. Simulation on the Rotational Vibration of Helical Gears in Consideration of the Tooth Separation Phenomenon (A New Stiffness Function of Helical Involute Tooth Pair). Journal of Mechanical Design 117, 460–469.

[4] Cappellini, N., Tamarozzi, T., Blockmans, B., Fiszer, J., Cosco, F., Desmet, W., 2018. Semi-analytic contact technique in a non-linear parametric model order reduction method for gear simulations. Meccanica 53(1), 49–75.

[5] Carbonelli, A., Rigaud, E., Perret-Liaudet, J., 2016. Vibro-Acoustic Analysis of Geared Systems-Predicting and Controlling the Whining Noise. Automotive NVH Technology (pp. 63-79). Springer, Cham .

[6] Catera, P.G., Gagliardi, F., Mundo, D., De Napoli, L., Matveeva, A., Farkas, L., 2017. Multi-scale modeling of triaxial braided composites for FE-based modal analysis of hybrid metal-composite gears. Composite structures 182, 116-123.

[7] Catera, P.G., Mundo, D., Treviso, A., Gagliardi, F., Visrolia, A., 2019. On the design and simulation of hybrid metal-composite gears. Applied Composite Materials 26(3), 817-833.

[8] Conry, T.F., Seireg, A., 1973. A Mathematical Programming Technique for the Evaluation of Load Distribution and Optimal Modifications for Gear Systems. Journal of Engineering for Industry 95, 1115–1122.

[9] Garambois, P., Perret-Liaudet, J., Rigaud, E., 2017. NVH robust optimization of gear macro and microgeometries using an efficient tooth contact model. Mechanism and Machine Theory 117, 78–95.

[10] Guilbert, B., Velex, P., Cutili, P., 2017. Static and dynamic analyses of thin-rimmed gears with holes. VDI, International Conference on Gears , 623–633.

[11] Guilbert, B., Velex, P., Cutili, P., 2019a. Quasi-static and dynamic analyses of thin-webbed high-speed gears: Centrifugal effect influence. Proceedings of the Institution of Mechanical Engineers, Part C: Journal of Mechanical Engineering Science 233(21-22), 7282-7291.

[12] Guilbert, B., Velex, P., Dureisseix, D., Cutili, P., 2019b. Modular hybrid models to simulate the static and dynamic behaviour of high-speed thin-rimmed gears. Journal of Sound and Vibration 438, 353-380.

[13] Guilbert, B., Velex, P., Dureisseix, D., Cutuli, P., 2016. A Mortar-Based Mesh Interface for Hybrid Finite-Element/Lumped-Parameter Gear Dynamic Models—Applications to Thin-Rimmed Geared Systems. Journal of Mechanical Design 138. Publisher: American Society of Mechanical Engineers Digital Collection.

[14] Hou, L., Lei, Y., Fu, Y., Hu, J., 2008. Effects of lightweight gear blank on noise, vibration and harshness for electric drive system in electric vehicles. Proceedings of the Institution of Mechanical Engineers, Part K: Journal of Multi-Body Dynamics 234(3), 447-464.

[15] Laursen, T.A., Maker, B.N., 1995. An augmented Lagrangian quasi-Newton solver for constrained nonlinear finite element applications. International Journal for Numerical Methods in Engineering 38(21), 3571–3590.

[16] Li, S., 2008. Experimental investigation and fem analysis of resonance frequency behavior of three-dimensional, thin-walled spur gears with a power-circulating test rig. Mechanism and machine theory 43(8), 934-963.

[17] Rigaud, E., Barday, D., . Modelling and analysis of static transmission error. effect of wheel body deformation and interactions between adjacent loaded teeth. Proceedings of the 4th World Congress on Gearing and Power Transmission, Paris, Vol. 3, 1999, pp.1961-1972 .

[18] Sainsot, P., Velex, P., Duverger, O., 2004. Contribution of gear body to tooth deflections - A new bidimensional analytical formula. J. Mech. Des. 126(4), 748–752.

[19] Shweiki, S., Palermo, A., Mundo, D., 2017. A Study on the Dynamic Behaviour of Lightweight Gears. Shock and Vibration, 2017 .

[20] Shweiki, S., Rezayat, A., Tamarozzi, T., Mundo, D., 2019. Transmission Error and strain analysis of lightweight gears by using a hybrid FE-analytical gear contact model. Mechanical Systems and Signal Processing 123, 573-590.

[21] Simo, J.C., Laursen, T.A., 1992. An augmented lagrangian treatment of contact problems involving friction. Computers & Structures 42(1), 97-116.

[22] Umezawa, K., Sato, T., Ishikawa, J., 1984. Simulation of rotational vibration of spur gear. Bulletin of JSME, 27(223), 102-109. .

[23] Weber, C., Banaschek, K., 1953. Formanderung und Profilrucknahme bei Gerad-und Schragverzahnten Antriebstechnik. Vieweg, Braunschweig, 11, 4.

[24] Welbourn, D.B., 1979. Fundamental knowledge of gear noise: a survey. No. IMechE-C117/79.

[25] Wriggers, P., 2006a. Discretization, Large Deformation Contact. Computational Contact Mechanics (pp. 225-307). Springer, Berlin, Heidelberg .

[26] Wriggers, P., 2006b. Discretization of the Continuum. In Computational Contact Mechanics (pp. 157-182). Springer, Berlin, Heidelberg .

[27] Wriggers, P., 2006c. Introduction to Contact Mechanics. Computational Contact Mechanics (pp. 11-29). Springer, Berlin, Heidelberg .

[28] Özgüven, H., Houser, D.R., 1988. Mathematical models used in gear dynamics—A review. Journal of Sound and Vibration 121(3), 383–411.

CRediT authorship contribution statement

Y. Benaïcha: Conceptualization, Methodology, Software, Validation, Investigation, Writing - Original Draft, Writing - Review and Editing, Visualization. **A. Mélot:** Conceptualization, Validation, Investigation, Data Curation, Writ-

ing - Review & Editing. **E. Rigaud:** Conceptualization, Supervision, Writing - Review & Editing. **J-D. Beley:** Conceptualization, Supervision, Funding acquisition, Writing - Review & Editing. **F. Thouverez:** Conceptualization, Supervision, Funding acquisition, Writing - Review & Editing. **J. Perret-Liaudet:** Conceptualization, Supervision, Funding acquisition, Writing - Review & Editing.

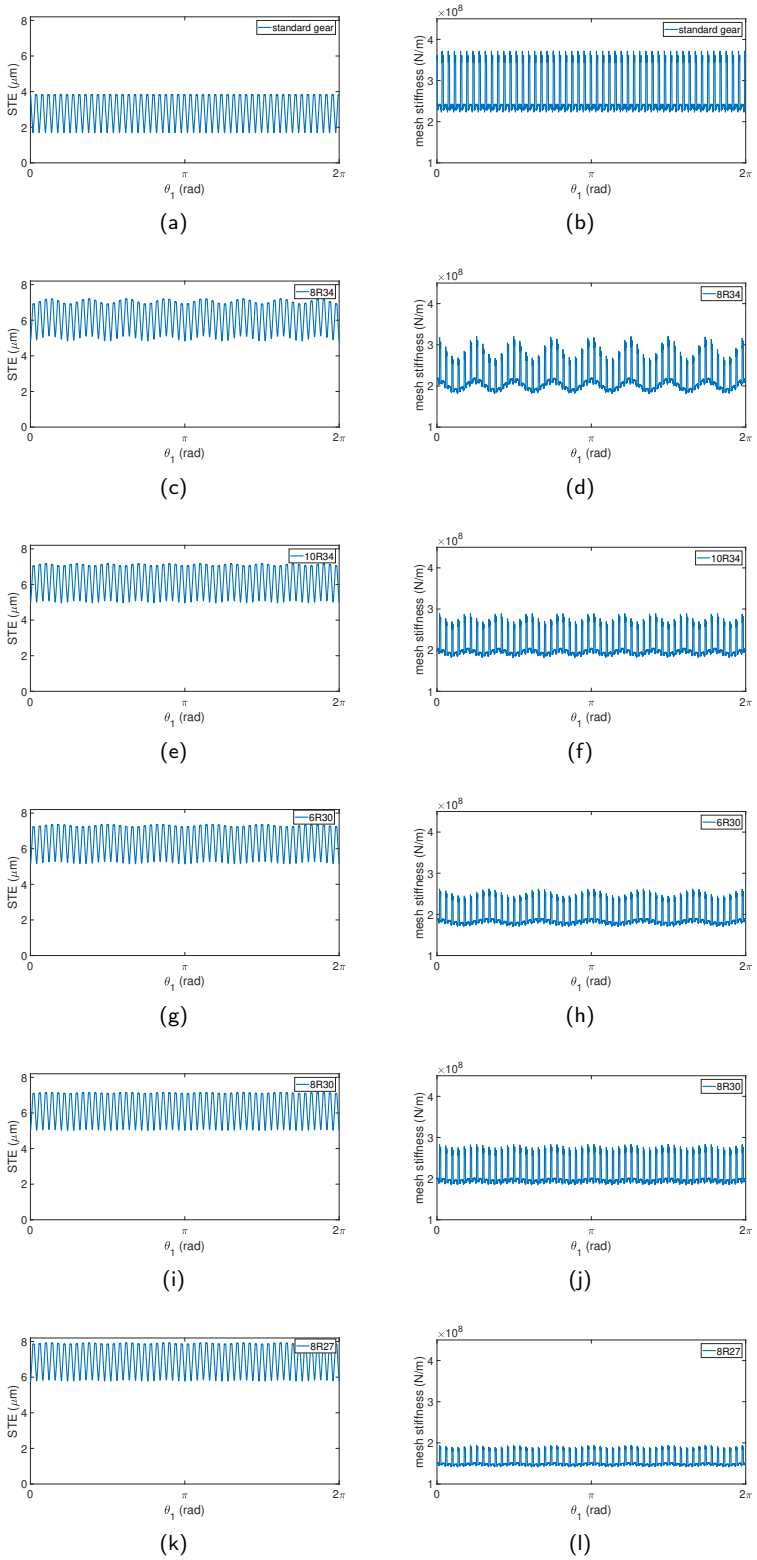

Figure 10: Time evolution of the STE and the mesh stiffness for an output torque $T = 20\,\mathrm{N\,m}$: (a,b) standard gear, (c,d) case 8R34, (e,f) case 10R34, (g,h) case 6R30, (i,j) case 8R30, (k,l) case 8R27.

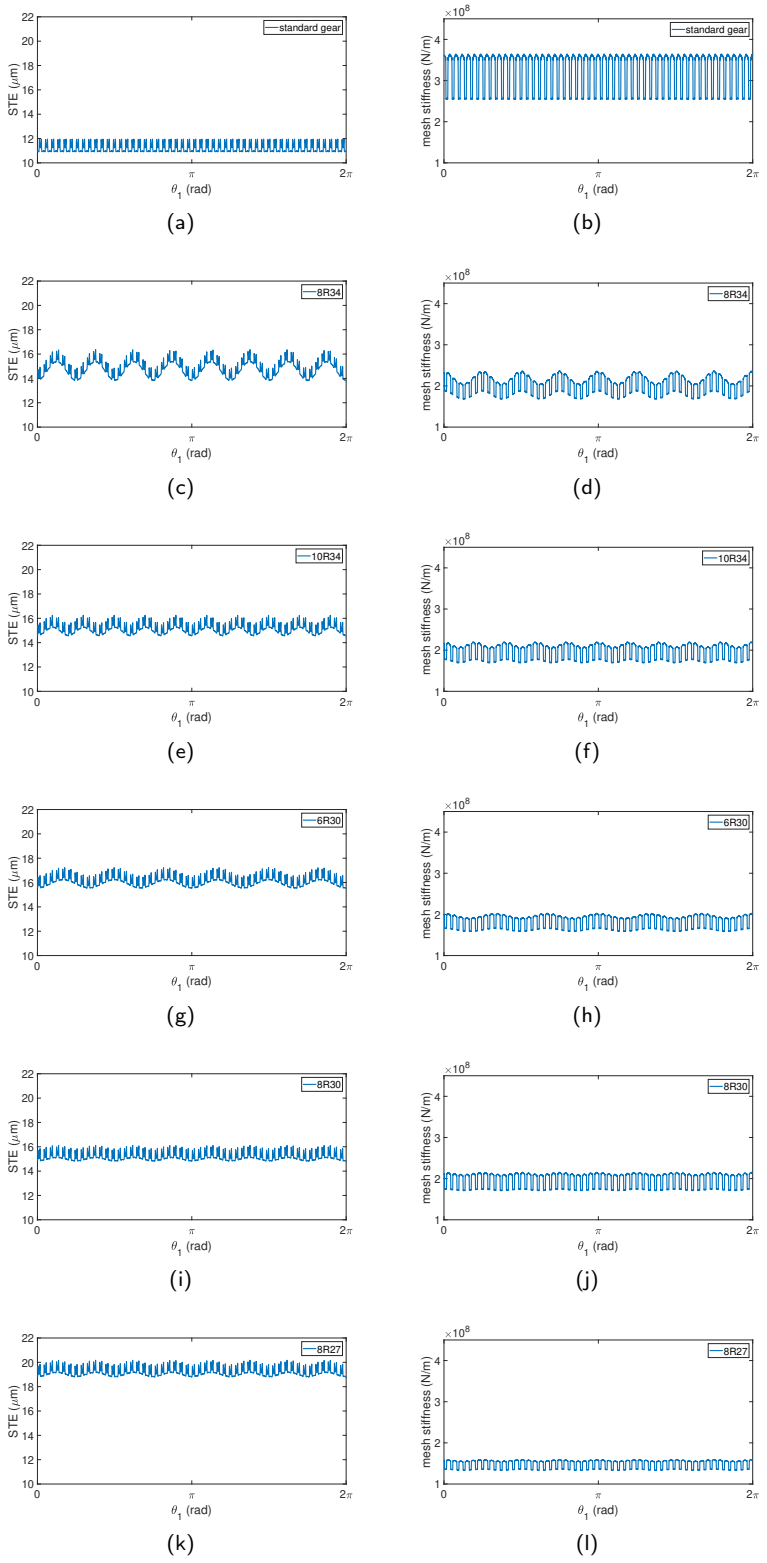

Figure 11: Time evolution of the STE and the mesh stiffness for an output torque $T = 115\,\mathrm{N\,m}$: (a,b) standard gear, (c,d) case 8R34, (e,f) case 10R34, (g,h) case 6R30, (i,j) case 8R30, (k,l) case 8R27.